Mol. Cryst. Liq. Cryst., Vol. 435, pp. 243/[903]–253/[913], 2005

ISSN: 1542-1406 print/1563-5287 online
DOI: 10.1080/15421400590956315

Taylor & Francis
Taylor & Francis Group

Square Patterns and their Dynamics in Electroconvection

Elbieta Kochowska
On leave from Henryk Niewodniczanski Institute of Nuclear Physics, Polish Academy of Sciences, Krakow, Poland

Nándor Éber
Ágnes Buka
Research Institute for Solid State Physics and Optics, Hungarian Academy of Sciences, Budapest, Hungary

Wojciech Otowski
On leave from Tadeusz Kosciuszko Cracow University of Technology, Krakow, Poland

Characteristics of electroconvection patterns have been studied in a homeotropic nematic liquid crystal with unusual combination of material parameters (negative conductivity and positive dielectric permittivity anisotropies). The morphological phase diagram has been explored. Two distinct types of pattern dynamics have been detected: losing autocorrelation of the pattern during temporal evolution due to spatio-temporal chaos at onset and domain coarsening of a grid pattern.

Keywords: coarsening; electroconvection; nematic liquid crystal; pattern formation

INTRODUCTION

Complex patterns observed in nature have attracted a considerable interest recently [1–4]. The formation of such patterns is usually associated with the instabilities of systems occurring under non-equilibrium conditions. The patterns observed may have very complicated

We wish to thank Gerhard Pelzl for providing the substance and Istvan Janossy for useful discussions. Financial support by the EU Research Training Network PHYNECS (EU-HPCF-CT-2002-00312), the Hungarian Research Grants OTKA-T031808 and OTKA-T037336 are gratefully acknowledged.

Address correspondence to Nándor Éber, Research Institute for Solid State Physics and Optics, Hungarian Academy of Sciences, H-1525 Budapest, P.O.B. 49, Hungary. E-mail: eber@szfki.hu

BACK TO CONTENTS

spatiotemporal behavior. A spectacular example of such phenomena is electroconvection (EC) in nematic liquid crystals (NLCs).

EC is typically observed in nematics possessing negative dielectric and positive conductivity anisotropies ($\varepsilon_a < 0,\ \sigma_a > 0$). Depending on easily variable control parameters (as the rms value and the frequency of the applied voltage) a rich morphology of patterns can be created. The preferred direction (x) defined by the surfaces (x-y plane) in planarly oriented cells results in well ordered roll patterns at the onset which are either stationary or move with a constant velocity (traveling waves), both have long correlation times. Correlation is typically lost faster at higher voltages where the pattern becomes dynamic due to the formation and motion of defects (dislocations) marking the path to chaos.

In contrast to the planar case, in homeotropically oriented cells EC is a secondary bifurcation occurring above a bend Freedericksz transition. In the Freedericksz distorted state the director bends away from z towards an arbitrary direction in the x-y plane and breaks the rotational symmetry of the homeotropic arrangement spontaneously. The in-plane director $\mathbf{c}$ is not prescribed externally (when no magnetic field is applied) thus $\mathbf{c}$ is a slowly varying function of x and y. This director distribution serves as a ground state with a Goldstone mode of slow dynamics and zero growth rate which interacts with the EC patterning mode at its onset [5]. Consequently one obtains spatio-temporal chaos (STC), often called soft mode turbulence [6], already at the onset of EC. This type of chaotic behavior has been devoted considerable attention to in recent years, both theoretically [5] and experimentally [7–9].

There exist, however, a few nematic liquid crystals which have $\varepsilon_a > 0,\ \sigma_a < 0$ (i.e., opposite signs of the anisotropies compared to the NLCs mentioned above). It has been hinted in the literature [10] that these substances may also exhibit electrohydrodynamic instabilities. Recently it has actually been proved [11,12] that at homeotropic orientation of NLCs with such an unusual combination of the material parameters the basic Carr-Helfrich mechanism of EC is fully operational, consequently it facilitates a direct transition from the undistorted homeotropic state to the electroconvecting one, without the necessity (and existence) of a preceding Freedericksz transition. Thus the azimuthal degeneracy due to the surface alignment is broken during the onset of the EC instability which classifies this system to another symmetry class.

In this paper we present a detailed analysis of the pattern morphology and the dynamic response of such an unconventional NLC.

BACK TO CONTENTS

EXPERIMENTAL SETUP

The experiments were done in the nematic phase of a "swallow-tailed" compound, p-(nitrobenzyloxy)-biphenyl [13]. The phase sequence is as follows: I–110°C–N–94°C–Sm C–75°C–Sm F–(66.5°C–Sm X)–69°C–Cr. The structure of the monotropic (showing up only on cooling) smectic X phase below the smectic F has not been identified. The substance has $\varepsilon_a > 0$ and $\sigma_a > 0$ in the whole nematic range [11].

Ready made homeotropic cells of various thicknesses ($d = 9$, 11 and 15 μm) were used in the conventional sandwich geometry. The cells were driven by sinusoidal voltage. The patterns were observed with a Leica DM RXP polarizing microscope and the temperature was controlled using an Instec hot-stage with an accuracy of 0.05°C. EC measurements were carried out at 96°C and 98°C. The images were recorded by an Optronics MicroFire digital camera with 32 bit color depth and were stored with a spatial resolution of 50×1000 pixels for autocorrelation and 1200×1600 pixels for coarsening measurements respectively. For further processing the recorded snapshots were converted to 8 bit gray-scale images.

THE HOMEOTROPIC PHASE DIAGRAM

The conductive range up to the cutoff frequency ω_c has been studied where EC sets in directly from the homogeneous state via a forward bifurcation, in contrast to the conventional ($\sigma_a > 0$, $\varepsilon_a < 0$) homeotropic case. As the Freedericksz transition is absent, the rotational symmetry is broken only at the onset of EC, the director perturbation (bending away from z) is an inherent part of the EC mode.

The morphological phase diagram is depicted in Figure 1 where the threshold voltage U_c is plotted against the dimensionless frequency $\omega\tau_q$ ($\tau_q = \varepsilon_0\varepsilon_\perp/\sigma_\perp$ is the charge relaxation time). Undulated zig-zag (ZZ) rolls are observed at very low frequencies at onset [11]. Increasing the frequency the pattern consists of areas of regular rolls and overlapping regions with two almost orthogonal roll directions (squares) with a well defined wave number $q_c(\omega)$ (Fig. 2a). The structure as a whole is, however, disordered, there is a spatial variation of the direction of the wave vector as a consequence of the absence of a preferred direction in the x-y plane due to the homeotropic director anchoring. The size of the overlapping regions increases with the frequency up to a point ω^* with $\omega^*\tau_q = 0.56$ (the Lifshitz point) [11] above which only squares are seen. Their orientation preserves the undulated character of the rolls and the slow spatial variation in the x-y plane, therefore are called soft squares (Fig. 2b).

BACK TO CONTENTS

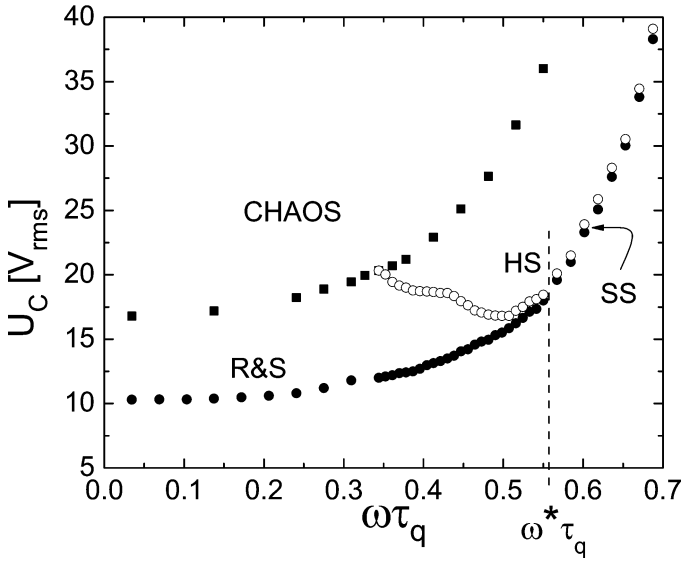

FIGURE 1 The morphological phase diagram at homeotropic orientation (R&S - rolls and squares, SS - soft squares, HS - hard squares).

The onset structure shows a slow, persisting dynamics for frequencies below ω^*. This involves a continuous change in the distribution of the direction of the wavevector. The ZZ character as well as the typical size of the domains persists with time. This dynamics will be addressed in the next section in more detail.

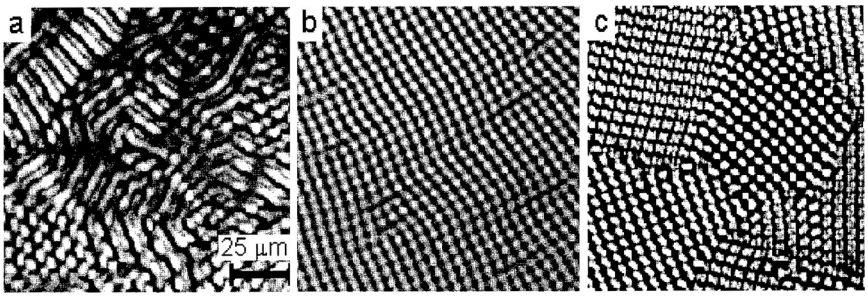

FIGURE 2 The morphologies observed a; - rolls and square ($\omega\tau_q = 0.233$, $\varepsilon = 0.19$), b; - soft squares ($\omega\tau_q = 0.612$, $\varepsilon = 0.04$), c; - hard squares ($\omega\tau_q = 0.583$, $\varepsilon = 0.47$).

BACK TO CONTENTS

Increasing the voltage above threshold at low frequencies we observe a shrinking of the size of the regular areas and the dynamics gets faster. The roll pattern gradually evolves into the turbulent regime with increasing voltage. At high frequencies the soft square pattern first becomes better oriented due to the reduction of the number of dislocations then (still at small ε) transforms into another pattern, which contains domains of well ordered square grids separated by sharp domain boundaries. This pattern, called hard squares (Fig. 2c), persists for high voltages, until the appearance of spatio-temporal chaos. There is an intermediate frequency range (below ω^*) where the same hard square pattern develops from the rolls and squares at increasing voltages as seen in Figure 1.

A quantitative comparison of the frequency dependence of the threshold voltage $U_c(\omega)$ and the onset wavenumber $q_c(\omega)$ with the standard theory [14] based on the Carr-Helfrich destabilization effect has yielded a very good agreement [11].

PATTERN DYNAMICS AT THRESHOLD

The time evolution of the patterns was studied as a function of frequency and the dimensionless control parameter $\varepsilon = (U_2/U_c^2) - 1$.

After application of the voltage corresponding to the chosen values of ε the pattern developed fully within a couple of seconds. While keeping ε constant subsequent two-dimensional snapshots have been recorded in every 1 s for a period of 300 s. An arbitrary line, the same in all pictures, was defined as the x-axis.

For quantitative characterization of the pattern dynamics a local autocorrelation function $C(x,t)$ of the intensity along the line $I(x,t)$ was computed according to the formula

$$C(x,t) = \frac{\langle (I(x,t+t_o) - \langle I(x,t+t_o)\rangle)(I(x,t_o) - \langle I(x,t_o)\rangle)\rangle}{D_{I(x,t+t_o)} \cdot D_{I(x,t_o)}}$$

where

$$D_{I(x,t+t_o)} = \langle (I(x,t+t_o) - \langle I(x,t+t_o)\rangle)^2\rangle \quad \text{and}$$
$$D_I(x,t_o) = \langle (I(x,t_o) - \langle I(x,t_o)\rangle)^2\rangle$$

are the standard deviations, and $\langle\cdot\rangle$ indicates averaging over the running variable t_o. The autocorrelation function $\hat{C}(t)$ was finally obtained by averaging over x.

Figure 3 shows the ε dependence of the autocorrelation function $\hat{C}(t)$ for one particular frequency ($\omega\tau_q = 0.047$) where rolls and squares

BACK TO CONTENTS

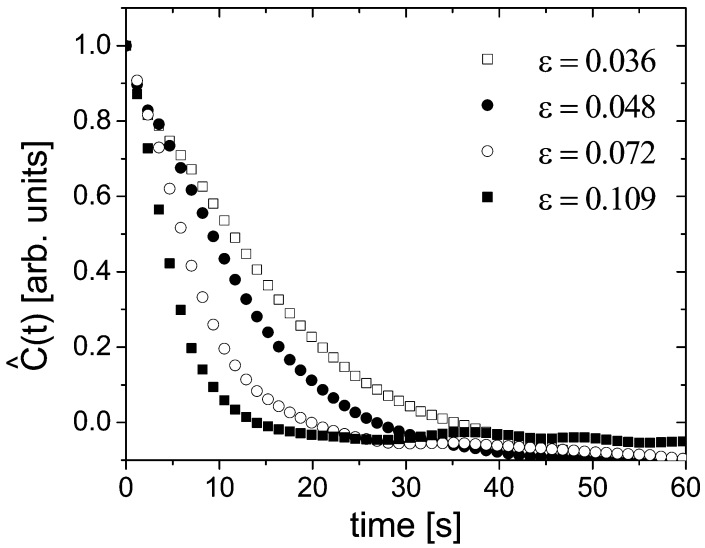

FIGURE 3 Autocorrelation function for $\omega\tau_q = 0.047$ for four different ε (0.035, 0.048, 0.072 and 0.109).

were observed. The autocorrelation function diminishes (what is expected for a developed chaotic regime) and its decay gets faster with increasing ε.

The correlation time τ_c was determined by least squares fitting of the autocorrelation functions with a single exponential decay $\hat{C}(t) = C_0 \cdot \exp(-t/\tau_c)$.

Figure 4 exhibits τ_c^{-1} versus ε for different frequencies covering two regions: the rolls and squares ($\omega\tau_q < 0.56$) and the squares only ($\omega\tau_q > 0.56$).

Experimental data may be well fitted by the law $\tau_c^{-1} \propto \varepsilon$ at small ω, which indicates a direct transition to STC from the homogeneous state [15]. At higher ω (above ω^*) the structure is stationary at onset up to $\varepsilon = 0.05$.

Increasing the frequency up to ω^* one observes rapidly decreasing slopes which implies an increase of the correlation times. For frequencies above ω^* the slope saturates. This behavior is similar to the results on conventional NLCs [9]. In Figure 5 the slope $(\tau_c\varepsilon)^{-1}$ is shown as a function of the reduced frequency ω/ω^*. For patterns dominated by rolls (low frequencies, $\omega/\omega^* < 0.5$) the slope is 5 times higher than for the squares ($\omega/\omega^* > 1$). For $\omega/\omega^* > 1$ the slope becomes almost frequency independent. Moreover, the pattern at onset seems to be stationary as indicated by the finite $\varepsilon \neq 0$ intersection of the last fitted

BACK TO CONTENTS

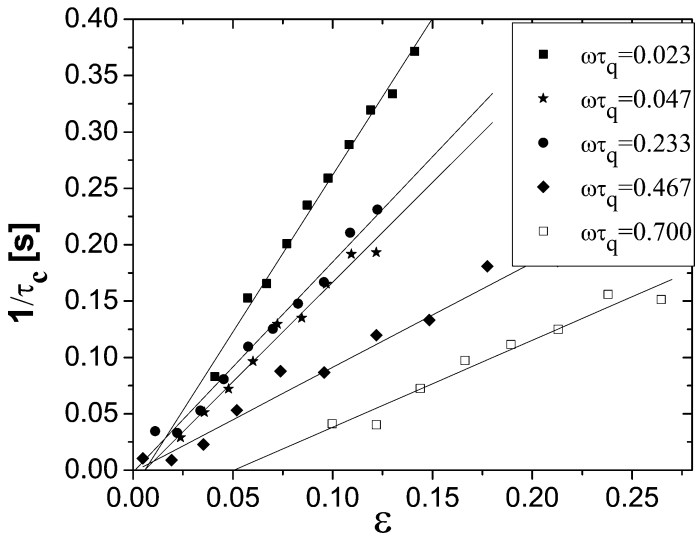

FIGURE 4 Inverse correlation time τ_c^{-1} versus ε.

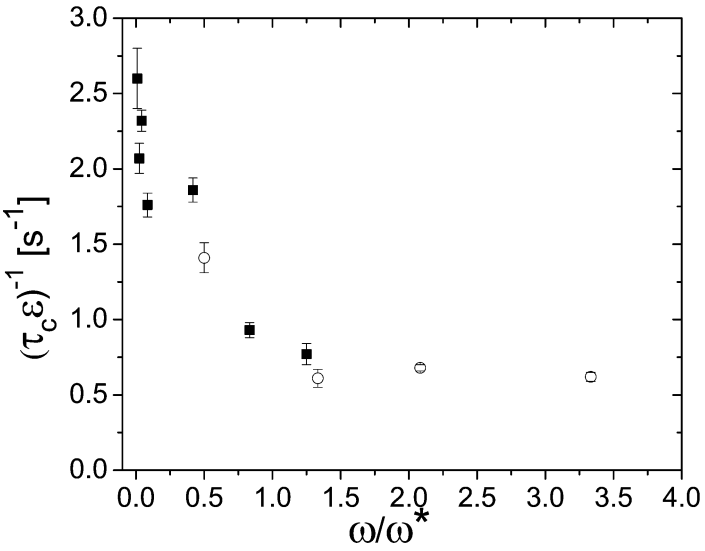

FIGURE 5 $(\tau_c\varepsilon)^{-1}$ as a function of the reduced frequency ω/ω^*. Solid squares refer to the results obtained for cells of thickness $\sim$15 μm and open squares for 9 μm (after re-scaling -see text).

BACK TO CONTENTS

line in Figure 4. Such behavior was also found in the normal roll regime of conventional NLCs [9]. Above $\omega/\omega^* > 1.25$ the measurement of $\tau_c(\varepsilon)$ meets difficulties as the soft squares exist in a narrow ε region only (see Fig. 1.). When $\omega\tau_q$ is slightly above 0.56 this ε existence range is about 0.2 but with increasing frequency this value decreases down to $\varepsilon \approx 0.05$, thus leaves too short ε range for reliably measuring $\tau_c(\varepsilon)$.

The characteristic time τ for the decay of the EC patterns is known to be thickness dependent. As a smaller thickness results in higher vertical (along z) director gradient and thus higher restoring torque, a faster relaxation is expected. Calculations predict $\tau \propto d^2$ dependence. Our situation is, however, more complicated as besides the thickness (which sets the wavelength as well) there is another characteristic length L_a for the azimuthal variation of the pattern orientation. Though no theoretical prediction is known yet for this geometry, one might expect that lateral director gradients should also affect the correlation time τ_c. Unfortunately L_a is out of control at present, so only the thickness dependence could be checked. Measurements on cells of three different thicknesses indicated a $\tau_c \propto d^2$ dependence thus indicating a dominance of d and negligible effect of L_a. In Figure 5 actually the results obtained for cells of $d_1 = 9\,\mu\text{m}$ (open circles) and $d_2 = 15\,\mu\text{m}$ (squares) are combined using a re-scaling by ${d_1}^2/{d_2}^2$ for $\tau_c(d_2)$.

COARSENING OF THE SQUARE DOMAINS

Losing correlation is not the only form of pattern dynamics. Occasionally, on the contrary, the pattern becomes more ordered in time, i.e., coarsens. This phenomenon has been observed in various systems, though only a few experiments on this field are known yet. They suggest that after a long time period the domain growth/shrinking can be characterized with a power-law, but the value of the growth exponent depends on the measurement scheme (on the choice of the measure of coarsening dynamics) [16–19] which may indicate the necessity of multiple correlation length scales [20]. Simulations of the potential and non-potential forms of the Swift-Hohenberg equation [16,18,21] have suggested a growth of $t^{1/5}$ for the characteristic length of domains obtained from a structure function $S(q)$ in the Fourier space [16,18]. However, in the case when the growth exponent is determined from the orientational correlation function, $t^{1/4}$ is expected for potential dynamics [16,18] and $t^{1/2}$ for a non-potential one [16].

Our electroconvecting nematic with its hard square pattern is another example of driven systems approaching a steady non-equilibrium state via coarsening. Jumping to the proper ε the pattern initially consists of small domains of perfectly ordered

BACK TO CONTENTS

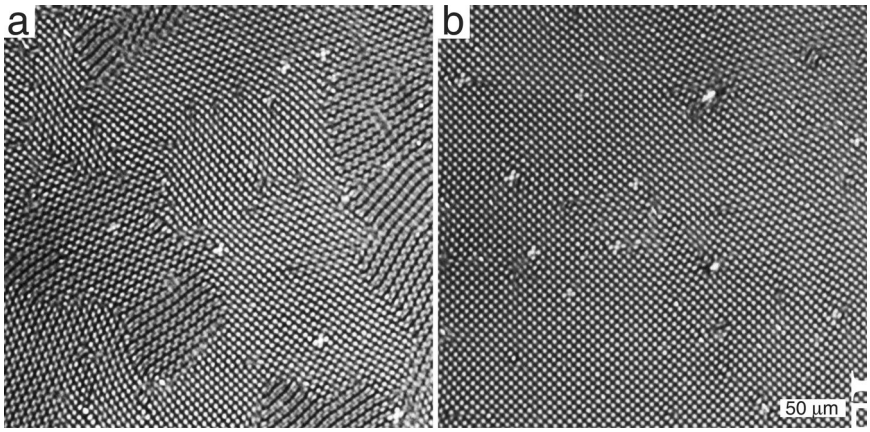

FIGURE 6 Coarsening of the square pattern at $T = 98^{\circ}C$, $\omega\tau_q = 1.63$, $\varepsilon = 0.21$. a; after 1 minute, b; after 89 minutes.

two-dimensional square grids with different orientation, separated by domain walls (Fig. 6a). The domain-walls are moving allowing the growth of some domains on the expense of shrinking ones over a period of minutes, resulting asymptotically in a very large ordered region (Fig. 6b).

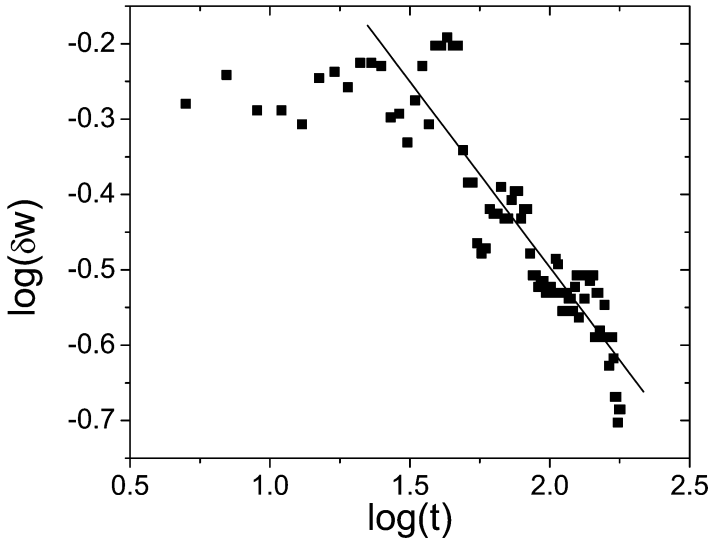

FIGURE 7 Plot of $\log(\delta w)$ versus $\log(t)$ for $\omega\tau_q = 1.167$ and $\varepsilon = 0.2$. The fitted line has a slope of -0.49 ± 0.02.

BACK TO CONTENTS

This evolution of patterns was monitored by recording a sequence of subsequent snapshot images and focusing on the orientation of the squares. A two-dimensional fast Fourier transformation (FFT) was applied to the same (512×512 pixels) region of all images and the azimuthal distribution was calculated at the radius q_c, the dominating wavenumber of the system. As a measure of the order the half width δw of the peak in the azimuthal distribution was taken.

Figure 7 exhibits a log-log plot of δw versus time for $\omega\tau_q = 1.167$ and $\varepsilon = 0.2$. Data indicate power law dependence after some initial transient period. Fitting a straight line for the final decade of time results in a slope of -0.49 ± 0.02, which indicates a growth exponent of 0.49 ± 0.02. After the time corresponding to the last data points the area selected for the FFT contained only two domains. Other measurements at different ω yielded similar values (-0.45 ± 0.02, -0.46 ± 0.06, -0.50 ± 0.10). This agrees quite well with the prediction for non-potential dynamics [16].

CONCLUSIONS

A direct transition from the homeotropic state to electroconvecting patterns has been observed in a nematic liquid crystal with $\varepsilon_a > 0$, $\sigma_a < 0$. Exploring the complete phase diagram in the (U, q) space three distinct morphologies, rolls and squares, soft squares and hard squares have been identified.

For the first type (frequencies below the Lifshitz point ω^*) the existence of spatio-temporal chaos at onset has been proved by measuring the autocorrelation of the pattern. In the case of the hard squares a domain coarsening has been observed which follows the $t^{1/2}$ law.

REFERENCES

[1] Cross, M. C. & Hohenberg, P. C. (1993). *Rev. Mod. Phys.*, *65*, 851, and references therein.
[2] Kai, S. (Ed.), *Pattern Formation in Complex Systems. Fluid Patterns, Liquid Crystals, Chemical Reactions*. World Scientific: (1992). Singapore.
[3] Walgraef, D. (1997). *Spatio-Temporal Pattern Formation. With Examples from Physics, Chemistry and Materials Science*, Springer: New York.
[4] Buka, A. & Kramer, L. (Eds.), (1996). *Pattern Formation in Liquid Crystals*. Springer: New York.
[5] Rossberg, A. G., Hertrich, A., Kramer, L., & Pesch, W. (1996). *Phys. Rev. Lett.*, *76*, 4729.
[6] Kai, S., Hayashi, K., & Hidaka, Y. (1996). *J. Phys. Chem.*, *100*, 19007.
[7] Hidaka, Y., Huh, J. H., Hayashi, K., Tribelsky, M. I., & Kai, S. (1997). *Phys. Rev. E*, *56*, R6256.

BACK TO CONTENTS

[8] Hidaka, Y., Huh, J. H., Hayashi, K., Tribelsky, M. I., & Kai, S. (1997). *J. Phys. Soc. Jpn.*, *66*, 3329.
[9] Toth, P., Buka, A., Peinke, J., & Kramer, L. (1998). *Phys. Rev. E*, *58*, 1983.
[10] de Gennes, P. G. & Prost, J. (1993). *The Physics of Liquid Crystals*, Clarendon Press: Oxford.
[11] Buka, A., Dressel, B., Otowski, W. *et al*. (2002). *Phys. Rev. E*, *66*, 051713/1–8.
[12] Buka, Á., Dressel, B., Kramer, L., & Pesch, W. *Phys. Rev. Lett.*, In press.
[13] Emmerling, U., Diele, S., Schmalfuss, H. *et al*. (1998). *Chem. Phys.*, *199*, 1529.
[14] Bodenschatz, E., Zimmermann, W., & Kramer, L. (1988). *J. Phys. (Paris)*, *49*, 1875.
[15] Hidaka, Y., Huh, J. H., Hayashi, K. I., & Kai, S. (1997). *Phys. Rev. E*, *56*, R6256.
[16] Christensen, J. J. & Bray, A. J. (1998). *Phys. Rev. E*, *5*, 5364.
[17] Purvis, L. & Dennin, M. (2001). *Phys. Rev. Lett.*, *86*, 5898.
[18] Cross, M. C. & Meiron, D. I. (1995). *Phys. Rev. Lett.*, *75*, 2152.
[19] Elder, K. R., Vinals, J., & Grant, M. (1992). *Phys. Rev. Lett.*, *68*, 3024.
[20] Paul M. R., Chiam K. H., Cross M. C., & Fischer P. F. to be published
[21] Qian, H. & Mazenko, G. F. (2003). *Phys. Rev. E*, *64*, 036102.

BACK TO CONTENTS